Distributed Source Model for Short-Range MIMO

by

Jeng-Shiann Jiang and Mary Ann Ingram

{jsjiang, mai}@ece.gatech.edu

School of Electrical and Computer Engineering
Georgia Institute of Technology

Distributed Source Model for Short-Range MIMO

Jeng-Shiann Jiang and Mary Ann Ingram
School of Electrical and Computer Engineering
Georgia Institute of Technology, Atlanta, GA 30332-0250, USA
jsjiang@ece.gatech.edu and mai@ece.gatech.edu

Abstract— **The plane-wave, or point-source, assumption has been used extensively in array signal processing, parameter estimation, and wireless channel modeling to simplify analysis. It is suitable for single-input-single-output (SISO) and single-input-multiple-output (SIMO) systems, because the rank of the channel matrix is one. However, for short-range multiple-input-multiple-output (MIMO) systems with line-of-sight (LOS), the point-source assumption affects the rank and singular value distribution of the MIMO channel matrix, and results in the underestimation of channel capacity, especially for element spacings exceeding a half wavelength. The short-range geometry could apply to many indoor wireless local area network (WLAN) applications. To avoid this under-estimation problem, the received signal phases must depend precisely on the distances between transmit and receive antenna elements. With this correction, the capacity of short-range LOS MIMO channels grows steadily as the element spacing exceeds half wavelength. We derive an empirically-based threshold distance below which the distributed source model is required for accurate performance estimation in ray tracing.**

Keywords- MIMO; channel capacity; line of sight; propagation; plane-wave assumption.

I. INTRODUCTION

Multiple-input-multiple-output (MIMO) transmission is an extremely spectrum-efficient technology that uses several antennas at both ends of the link [1,2]. However, it has been revealed that some factors such as the richness of the multipath, the correlation of the channel matrix, and the keyhole effect might degrade its performance significantly in the real environment [3,4]. Two groups [5,6] have attempted to estimate the path parameters of the MIMO channel for the purpose of reconstructing the matrix of MIMO channel gains for arbitrary array geometries. The path parameters include the angles of departure and arrival at the transmitter and receiver arrays, respectively. However, both groups found that the capacity of the reconstructed MIMO channels was less than the directly measured capacity. In this paper we show that, at least in [6], a major reason for the discrepancy is incorrect modeling of the line-of-sight (LOS). Specifically, we find that computing received signal phases based on the precise distances between transmit and receive antennas is necessary to remove the discrepancy. This way of modeling the LOS, which we call the "distributed-source model" gives "richness" to even a free-space MIMO channel.

This observation was made by Driessen and Foschini [7], where particular geometries were sought that could yield channel matrices with full rank. The authors in [8] investigated this phenomenon by simulating the free space and two-path channels, but only two orientations of the arrays were considered. They validated the phenomenon over measured channels in a parking lot with fixed antenna spacing (half wavelength). Also using the distributed model, the authors in [9] showed that the capacity was sensitive to element spacing in free-space and Rician fading channels with various K-factors, which were simulated by adding Rayleigh-distributed random variables to the LOS component. They concluded that the sensitivity of capacity to the element spacing is significantly reduced when the K-factor is less than 10 dB.

In contrast to these previous works, this paper analyzes the performances of arrays with various orientations and elevation angles in free space channel and a square room with up to 20 reflections. In addition, we specify a threshold to determine whether the point-source model can be used without causing significant errors. Furthermore, this paper uses a measured indoor channel to show how the more precise LOS model narrows the gap between capacities of measured and reconstructed MIMO channels, especially for larger element spacing. Moreover, because the LOS path is much stronger than the multipath, and because LOS alone can provide substantial capacity, we conclude that special care should be taken when modeling the LOS in short-range MIMO links, even when there is plenty of multipath.

Other authors have considered the effect of element spacing on MIMO capacity. Increased capacity with increased element spacing in non-LOS (NLOS) channels has been observed in simulation of stochastic geometric models with angularly clustered multipath [10,11], and in ray tracing [12] because the increased spacing decorrelates the multipath fading. Others have analyzed short-range LOS MIMO links using ray tracing and concluded that capacity is either insensitive to spacing [13] or that half-wavelength spacing yields full capacity [14]. In [13], the point-source model is specified and in [14], the LOS model is not specified. In the context of these previous works, we first note that the LOS component is unfaded, therefore the spacing effects reported here are not because of decorrelation of fading. Secondly, as shown here, the conclusions about spacing that follow from the distributed model are different from those of [13] and [14]. Finally, in contrast to Driessen and Foschini [7], this paper considers the statistics of free-space short-range MIMO capacities for array geometries and random relative orientations that might be encountered in wireless local area network (WLAN) applications. The results suggest that larger element spacing could be very beneficial for indoor WLANs using MIMO.

The paper is organized as follows. In Section II, the free space channels are considered, and the discrepancy between the point and distributed-source models is demonstrated for

This research was supported in part by the National Science Foundation under Grant No. CCR-0121565, and in part by the Georgia Tech Broadband Institute (GTBI).

variations in direction-of-arrival (DOA), direction-of-departure (DOD), antenna spacing, and distance between transmit array (Tx) and receive array (Rx). In Section III, we use ray-tracing to simulate the multipaths with up to 20 reflections in a square room. The performances of both models are compared by Monte-Carlo approach. In Section IV, we briefly describe our MIMO measurement system and show the measurement results to validate the importance of the distributed-source model in the MIMO channel modeling. A short conclusion is provided in Section V.

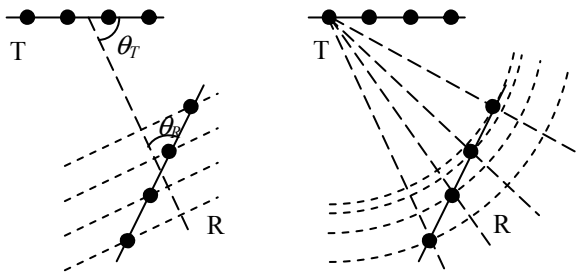

Figure 1: (a) Point-source model. (b) Distributed-source model.

II. FREE SPACE CHANNEL

The point- and distributed-source models for a (4,4) MIMO system are illustrated in Figure 1. This point-source model assumes the Tx and Rx arrays are point sources and the incident signal is a plane wave, which means the DOD or θ_T, (DOA or θ_R) is the same for all the elements in the Tx (Rx). However, when the distance between Tx and Rx is short, or the array size is large, the waves are more appropriately considered as spherical, which is the basis for the distributed-source model in the paper. Assuming each antenna element is in the far field of the other, and that the antenna elements are isotropic, the channel response between any two antennas is calculated according to the formula:

$$h \propto \frac{e^{-j\frac{2\pi D}{\lambda}}}{D}, \qquad (1)$$

where λ is the wavelength of the signal and D is the distance between the transmit and receive antenna pair [7]. In this section, we assume the LOS is the only path in the channel. The open-loop capacity is calculated by [1]

$$C = \log_2 \left| I_{n_R} + (SNR / n_T) \cdot \mathbf{H}\mathbf{H}^{\dagger} \right|, \qquad (2)$$

where n_T and n_R are the numbers of antennas at the transmitter and receiver sites, respectively, **H** is the MIMO complex channel matrix normalized such that the magnitude of each element has unit mean square value, SNR is the signal-to-noise ratio, and † stands for the complex conjugate transpose of the matrix. Using the point-source model in free space, the calculated capacity of the (4,4) MIMO system is 8.6475 bits/s/Hz for a SNR of 20 dB no matter how the DOA, DOD, the antenna spacing, and the array geometries are changed because the rank of the matrix is one. On the other hand, the maximum capacity is $\min(n_T,n_R)\log_2|1+SNR|$; this occurs when the channel matrix is orthogonal. For the (4,4) case, this maximum is 26.4 bits/s/Hz for SNR = 20 dB. In the following subsections, we will show that the maximum capacity is reached in free space over distances typically found in WLAN applications using the more precise distributed-source model.

A. The Azimuth Angle Of DOA And DOD

Assuming the distance between the Tx and Rx, denoted as the T-R distance, is 100λ, the calculated MIMO capacities with various azimuth angles of DOA, DOD, and antenna spacing using the distributed-source model are shown in Figure 2. Figure 2 demonstrates the MIMO capacities with antenna spacing 1λ and 7λ. First, we observe that this capacity varies with DOA and DOD. Compared to the capacity of 8.6475 bits/s/Hz in point-source model, these capacities are larger by 1.5 to 20 bits/s/Hz. The difference is increased with the increase of antenna spacing. In the distributed-source model, the minimum capacity occurred when either θ_T or θ_R are 0° or 180°. On the other hand, the maximum capacity happens when θ_T and θ_R are 90° when antenna spacing is less than 7λ. When the spacing exceeds 7λ, some ripples appear as θ_T and θ_R are close to 90°. The distribution of the capacity is symmetric with the point (θ_T, θ_R)=(90°, 90°).

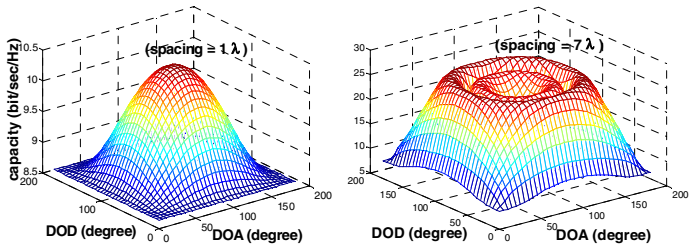

Figure 2: Change of MIMO capacity with DOA and DOD. The T-R distance is 100 λ, and the SNR is 20 dB.

Notice that when (θ_T, θ_R)=(0°, 0°), the rank of the channel matrix is only one because the DOA for all Rx array elements and the DOD for the Tx array elements are the same. When (θ_T, θ_R)=(90°, 0°), the rank of the channel matrix is two because the distances from the first Tx antenna to the Rx array elements are the same as that from the 4th antenna, and the distance from 2nd and 3rd antenna to the Rx array elements are also the same. In addition, when θ_T or θ_R is close to 0° or 180°, difference of the actual DOA and DOD of different elements is small, which results in the channel matrix with one large singular value and hence small channel capacity.

The differences between the DOAs and the differences between the DODs of different elements become smaller when the T-R distance is increased. Therefore, it is important to realize how the capacity is reduced with the increase of the T-R distance. Fixing (θ_T, θ_R)=(90°, 90°) and antenna spacing = 1λ, the simulated capacity for various distances and SNRs is shown in Figure 3. We observe that the capacity decreases with the increase of the distance primarily because the angular spread of the LOS paths is reduced. With large distance, the capacity approaches asymptotically the point-source capacity. We stress that the decrease has nothing to do with the path loss because the channel matrix is normalized in the capacity calculation. On the other hand, the difference between the maximum and minimum capacity is more significant when SNR is higher.

The difference is 8 bits/s/Hz when SNR = 10 dB, but it is raised to 35 bits/s/Hz when SNR = 40 dB.

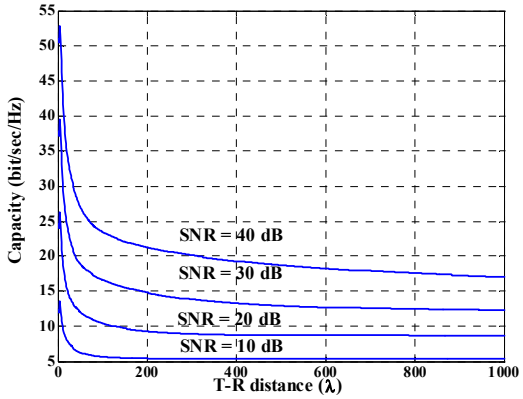

Figure 3: MIMO capacity with various distance and SNR.

It may seem that the T-R distance should be normalized by the antenna spacing because this would preserve the angular width of one array as viewed by the other array. However, the relative phases at the antenna elements and therefore the capacities still depend on the inter-element distances in terms of wavelength. Therefore, array-to-array geometries that are simply scaled versions of each other do not generally yield the same capacity.

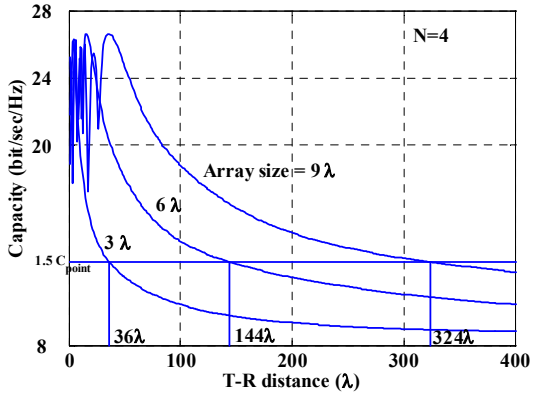

Figure 4: Capacity versus array size and T-R distance. The threshold distance to determine the appropriateness of point-source model.

A distance threshold that determines when the distributed model should be used can be determined empirically. To get this, we identify the distance R_{th}, below which the distributed-source capacity is greater than 1.5 times the point-source model for a given array size. In other words, the capacity underestimation error is 50% at this distance when point-source model is used, and this error increases dramatically when the T-R distance is shorter than R_{th}. As shown in Figure 4, for the array sizes 3λ, 6λ, and 9λ, the corresponding threshold distances are 36λ, 144λ, and 324λ, respectively, in the simulation when the number of antennas is 4. The relationship that fits this data is $R_{th} = 4L^2$, where L is the array size in units of wavelength. Given the formula $R_{th} = \alpha L^2$, the value of α ranges from 3.75 to 4.4 for the number of antennas from 3 to 16. Therefore, $4L^2$ is a reasonable threshold distance. For example, when the center frequency is 5.8GHz and the number of antennas is 4, the threshold distances are around 1.86m, 7m, and 16.8m for the antenna spacings 1λ, 2λ, and 3λ, respectively. This implies that the distributed-source model should be used, and antenna spacings in excess of 1λ should be considered, for MIMO in indoor wireless LAN applications where the client platform, such as a laptop computer or flat-panel TV, might support larger element spacings.

It is interesting to note that this threshold distance to distinguish the point- and distributed-source models is similar to the threshold $R = 2L^2$, which is used to distinguish the near and far field (L denotes the antenna size in this case) [15].

B. *Elevation angle*

Since the MIMO capacity depends on the difference among the DOAs and the differences among the DODs for different elements, the performance can be affected by changing the elevation angle. As illustrated in Figure 5(a), when the azimuth angles are (θ_T, θ_R)=(0°, 0°) and the elevation angle is ϕ = 90° (Tx and Rx are end to end on the same plane), the system has minimum capacity. If the elevation angle is then changed to 45°, as shown in Figure 5(b), the capacity would be the same with the condition when (θ_T, θ_R)=(45°, 45°) and ϕ = 90°.

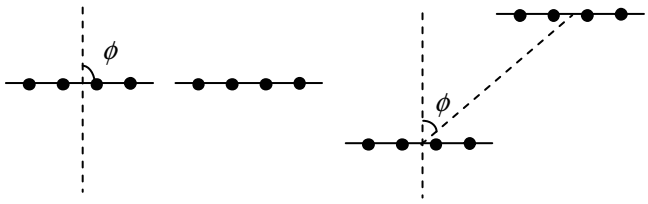

(a) ϕ = 90° (b) ϕ = 45°

Figure 5: MIMO system with the same azimuth angle but different elevation angles.

When the elevation angle is ϕ = 0°, the Rx and Tx will be broadside to each other when (θ_T, θ_R)=(0°,0°); this geometry is the same as when (θ_T, θ_R)=(90°, 90°) and ϕ = 90°, which has the maximum capacity. The MIMO system capacity with various azimuth angles and elevation angles are demonstrated in Figure 6. Although the maximum and minimum capacities are close for various elevation angles, the MIMO channel with ϕ = 0° has the best average capacity. The results suggest that the Tx should be placed on the ceiling to decrease the elevation angle and increase the performance when the LOS is available and dominates the performance of the MIMO system.

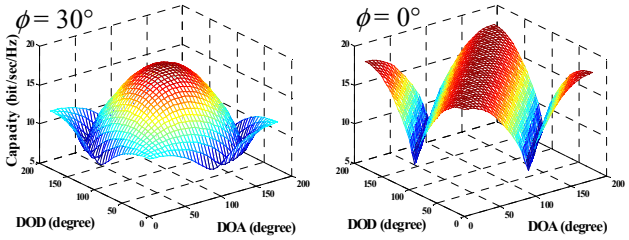

Figure 6: MIMO system with various elevation angles. The T-R distance is 100 λ, the antenna spacing is 3λ, and the SNR is 20 dB.

C. *Array geometry*

The MIMO capacity also changes with the array geometry in free space when the distributed-source model is utilized. For instance, the channel with (θ_T, θ_R)=(0°, 0°) is the same as (θ_T, θ_R)=(90°,90°) when the transmitter and receiver both have

uniform rectangular arrays (URAs); however, these two (θ_T, θ_R) conditions correspond to the maximum and minimum capacities, respectively, when the ULAs are employed instead.

The URAs eliminate the situations where the rank of the channel matrix is only one or two, which can occur with ULAs. Compared to the ULA MIMO system, the variance of the capacity is very small, which means the URA MIMO system has more stable performance.

With the distributed-source model, we can compare the capacities of various array geometries. In Figure 7, we compare the performance of the arrays with different combinations, including ULA-ULA, ULA-URA, and URA-URA. The SNR is 20 dB, the element spacing is 2λ, and four ranges are considered, which yield values of T-R distance-to-element spacing ratio (DSR) of 100, 50, 20, and 10, as indicated in Figure 7. The average and standard deviation of the capacity are derived assuming the DOA and DOD are independent and both uniformly distributed over [0°, 180°]. In Figure 7, the length of the vertical line on each curve represents the standard deviation for the corresponding array arrangement and elevation angle. Note that the vertical scales of small DSR (10 and 20) are nearly twice those of large ratios (50 and 100).

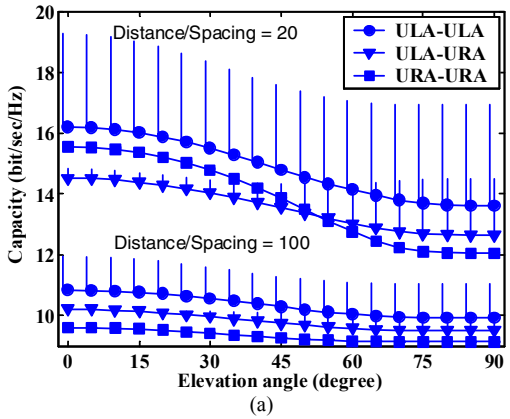

(a)

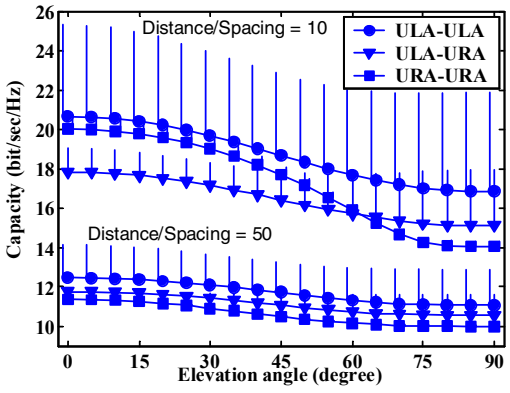

(b)

Figure 7: The average and standard deviation of MIMO capacity of different array geometries: The distance-to-spacing ratios are (a) 100 and 20 (b) 50 and 10.

The ULA-ULA combination has the best average capacity for all cases, but its standard deviation is also the largest. The average capacity of URA-URA surpasses ULA-URA at most elevation angles when the DSR is less than 20 (i.e., for the shorter ranges). In all cases, the capacity achieves its maximum when the elevation angle is close to 0°. The elevation angle effect is more significant when the DSR is smaller. For example, when the DSR is 10, the maximum difference of the capacity is about 6 bits/s/Hz for URA-URA system. In addition, URA-URA has the feature of smallest variance compared with the other two combinations. In other words, the performance of URA-URA is more robust. Finally, we note that on the average, element spacing improves the normalized URA-URA channel by about the same amount, 10 bits/s/Hz, at the zero elevation as it does the ULA-ULA configuration.

III. CHANNELS WITH MULTIPATH

In the previous section, we considered the capacity of the MIMO link when the LOS is the only path in the channel. However, in reality there are multiple paths caused by the reflection, refraction, and scattering of the objects around the antennas. In this section, we compare the point- and distributed-source models in a square room using 2D ray tracing with the image method [16]. The reflection coefficient ρ of the walls can be expressed as [13,15]

$$\rho = \frac{\sqrt{\varepsilon - \sin^2\theta} - \varepsilon\cos\theta}{\sqrt{\varepsilon - \sin^2\theta} + \varepsilon\cos\theta}, \tag{3}$$

where ε is the relative permittivity of the wall, and θ is the incident angle. In the simulation, we assume ε = 5 and the room size is (160 × 160) λ. The SNR is 20 dB. When the frequency is 5.8 GHz, the room size is about (8m × 8m), which is the size of a typical office. Both Tx and Rx are 4-element ULAs, and they are located at random and in the same horizontal plane in the room. The orientation of the array is also uniformly distributed in azimuth over [0°, 180°]. Up to 20 reflections are considered, so the number of total paths is 840. The number of trials in the simulation is 5000.

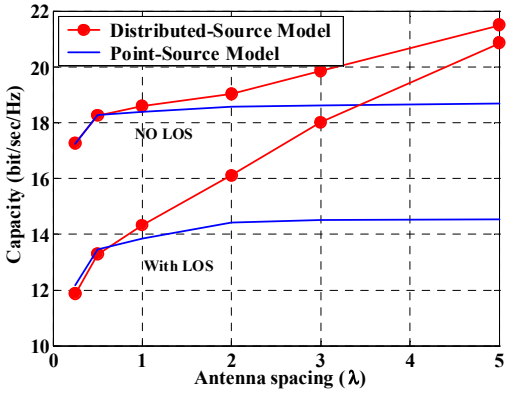

Figure 8: Comparison of the average capacities.

Figure 8 shows the average capacities for normalized channel matrices with and without the distributed-source model. We observe that the discrepancy between these two models is negligible when the antenna spacing is less than one wavelength, but the error increases with the increase in antenna spacing. We observe the difference of the average capacity is about 3 bits/s/Hz at 5λ when LOS is not included. If the LOS is

included in the simulations, bringing the total number of paths to 841, the discrepancy increases to 6.2 bits/s/Hz. In the point-source model, the average capacity tends to saturate when the antenna spacing exceeds 1 λ, whereas in the distributed-source model, the performance improves continuously for antenna spacing up to 5 λ.

IV. VALIDATION WITH MEASUREMENT

Next we use measured data acquired in the Smart Antenna Research Laboratory (SARL) at the Georgia Institute of Technology to compare the capacities of measured channels and the channels reconstructed with both point and distributed-source models based on estimated parameters. The testbed is composed of two parts: (1) the 3-D actuator system, which moves the antenna to pre-programmed locations to form a virtual array (there are two of these systems, one at each end of the link), and (2) the HP85301B antenna pattern measurement system, which captures the frequency response of the channel. The details of the measurement system are provided in [6].

The measurements were taken in the main room of the Smart Antenna research Laboratory, which is approximately $7\times4\times3m^3$, and which contains desks and 1.5m-high partitions. The T-R distance was 2.56m, and the link was in the center of the open area. In the experiment, two separate measurements were conducted; one for parameter estimation, and the other for direct capacity measurement. In the path parameter estimation, the arrays at both ends are (4×4×3) uniform cubicle arrays with antenna spacing 0.48 λ. 401 samples are measured from 5.55 – 6.05 GHz with the stepped-frequency method to achieve the temporal resolution of 2 *ns* and an unambiguous delay of 800 *n*s. Spatial and frequency smoothing is achieved by averaging the correlation matrices derived from the subarrays. The subarray sizes used in the estimation are (3×3×2) and (3×3×2), for DOA and DOD, respectively. The delay is estimated by unitary ESPRIT, and the DOA and DOD are jointly estimated by multi-dimensional ESPRIT [6,17,18]. According to the parameter estimation results, the channel is dominated by the LOS and the single-bounce paths. The power of LOS is 10 dB stronger than the 2nd strongest path.

In the capacity measurement, the Tx array is a 5-element ULA, while the Rx array is a (5×5) URA. To obtain independent outcomes for the flat-fading capacity cumulative distribution function (CDF), the frequency spacing is set to 10 MHz. Accordingly, there are 51 samples over 500 MHz bandwidth. To get spatial samples of capacity, subarrays with different array shapes and spacings are extracted from the 5-element ULA and (5×5) URA. With this arrangement, we may extract a total of 1632 outcomes of MIMO channel matrices when the (Tx, Rx) subarray setting is the (4,2×2) ULA-URA combination, and 1020 outcomes when the setting is (4,4) ULA-ULA for capacity CDF calculation. When the array arrangement is ULA-ULA, the Tx and Rx could be either orthogonal or parallel; accordingly, we may measure the channel capacities of three different array geometries.

Figure 9(a) shows the cumulative distribution functions (CDFs) of the measured capacities of the (4,4) MIMO system, with the arrays broadside to each other as shown by the large dots, for various antenna spacings. We observe that when the antenna spacing is increased from 0.5λ to 3λ, the S-shaped CDFs move to the right by about 7 bit/s/Hz, corresponding to an increase in the median capacity of about 23%.

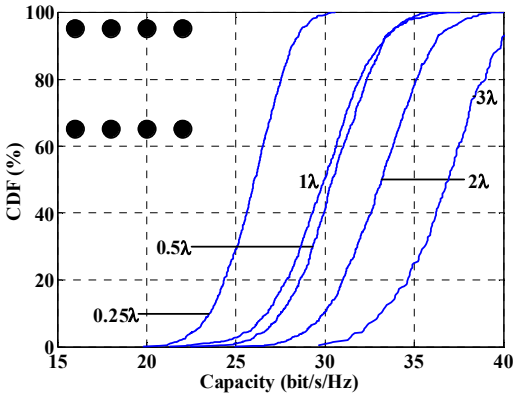

(a) Measured capacity

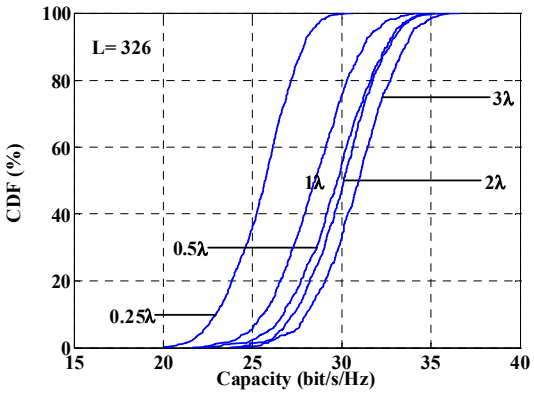

(b) Reconstructed capacity using point-source model

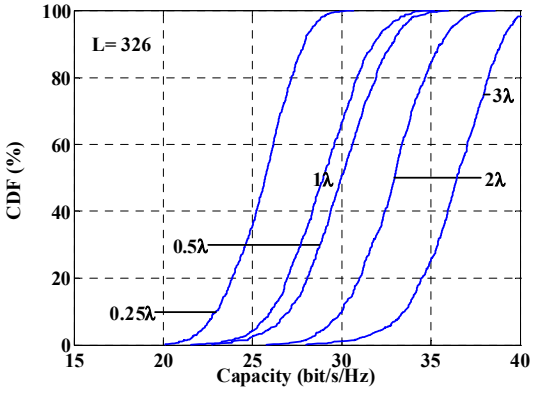

(c) Reconstructed capacity using distributed-source model

Figure 9: Comparison of measured and estimated capacities: (a) Measured capacity. (b) Reconstructed capacity using point-source model (c) Reconstructed capacity using distributed-source model.

Figure 9(b) shows the capacities of the reconstructed matrices using the estimated parameters and the point-source model. The estimated number of paths L is 326. We observe that the point-source model obviously underestimates the measured capacity, especially when the antenna spacing is larger than 1λ. When the antenna spacing is 3λ, the discrepancy between the median capacities is as large as 6 bit/s/Hz. In contrast, the estimated capacity based on

distributed-source model, as shown in Figure 9(c), has much better agreement with the measured capacity. Notice the distributed-source can be applied only to the LOS path because the intermittent reflections of the other NLOS paths cannot be obtained from the estimation.

Figure 10 shows the mean capacity for the directly measured channels minus the mean capacity of the reconstructed channel as a function of the LOS model, the element spacing, and the array geometries. Unless otherwise specified, the geometries are (ULA,ULA). The URA geometries is the (4, 2×2) system, and the ULA geometries are (4,4) MIMO systems where the ULAs are either parallel or orthogonal to each other. In all cases, the difference increases with the antenna spacing when point-source model is used, while the difference is maintained at a low level for various antenna spacings when distributed-source model is applied. We observe that the point-source model obviously underestimates the measured capacity, especially when the antenna spacing is larger than 1λ. The largest error of 6 bit/s/Hz occurs for 3λ spacing for parallel ULAs. In contrast, the estimated capacity based on distributed-source model has much better agreement with the measured capacity.

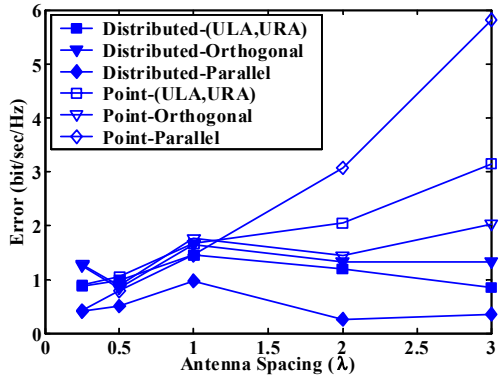

Figure 10: Comparison of capacity estimation error with point- and distributed-source models.

V. CONCLUSIONS

In this paper, we have considered the pure LOS channel as well as the channels with multipath, and have estimated the channel capacity based on ray-tracing methods and measured channels. We have shown that when the LOS is present the distributed-source model is more appropriate than the point-source model for MIMO systems when the T-R distance is short or the antenna spacing is large. A threshold distance is provided for linear arrays with up to 16 elements. We also show that, unlike the point-source model, the distributed-source model enables the performance of the short-range LOS MIMO system to be significantly improved by properly adjusting the DOA, DOD, and the array geometries. In particular, capacity can be dramatically improved by increasing the antenna spacing at both ends of the link. According to the simulations, better capacity can be achieved by placing the base station on the ceiling, provided the LOS is available. In the context of indoor WLANs, the results suggest that greater-than-single wavelength element spacing should be considered for non-handheld user platforms.

REFERENCES

[1] G.J. Foschini and M.J. Gans, "On limits of wireless communications in a fading environment when using multiple antennas," *Wireless Personal Communications*, pp.311-335, 1998.

[2] G.G. Raleigh and J.M. Cioffi, "Spatio-temporal coding for wireless communication," *IEEE Trans. Communications*, vol. 46, pp. 357-366, March 1998.

[3] D-S. Shiu, G.J., Foschini, M.J. Gans, and J.M. Kahn, "Fading correlation and its effect on the capacity of multielement antenna systems," *IEEE Trans. Communications*, vol. 48, pp. 502-513, March 2000.

[4] D. Chizhik, G.J. Foschini, M.J. Gans, R.A. Valenzuela, "Keyholes, correlations, and capacities of multielement transmit and receive antennas," *IEEE Trans. Wireless Communications*, vol. 1, pp. 361-368. Apr. 2002.

[5] A.F. Molisch, M. Steinbauer, M. Toeltsch, E. Bonek, R.S. Thoma, "Capacity of MIMO systems based on measured wireless channels," *IEEE Journal on Selected Areas in Comm*. Vol. 20, NO. 3, pp. 561-569, April 2002.

[6] J-S, Jiang, M. Ingram, "Path models and MIMO capacity for measured indoor channels at 5.8 GHz," *IEEE International Symposium on Antenna Technology and Applied Electromagnetics*, Aug. 2002.

[7] P.F. Driessen, G.J. Foschini, "On the capacity formula for multiple input-multiple output wireless channels: A geometric interpretation," *IEEE Trans. Communications*, vol. 47, pp. 173 – 176, Feb. 1999.

[8] P. Kyritsi, "MIMO capacity in free space and above perfect ground: Theory and experimental results," *IEEE Symposium on Personal, Indoor, and Mobile Radio Communications*, vol.1, pp. 182-186, Sep. 2002.

[9] A. Hutter, F. Platbrood, and J. Ayadi, "Analysis of MIMO capacity gains for indoor propagation channels with LOS component," *IEEE International Symposium on Personal, Indoor and Mobile Radio Communications*, vol. 3, pp. 1337-1341, Sep. 2002.

[10] D. Chizhik, F. Rashid-Farrokhi, J. Ling, and A. Lozano, "Antenna separation and capacity of BLAST in correlated channels," *IEEE Antenna and Propagation for Wireless Communications Conference*, pp. 183-185, 2003.

[11] K-H. Li, M.A. Ingram, A.V. Nguyen, "Impact of clustering in statistical indoor propagation models on link capacity," *IEEE Trans. on Communications,* pp. 521-523, Apr. 2002.

[12] C-N. Chuah, G.J. Foschini, R.A. Valenzuela, D. Chizhik, J. Ling, and J.M. Kahn, "Capacity growth of multi-element arrays in indoor and outdoor wireless channels," *IEEE Wireless Communications and Networking Conference*, vol. 3, pp. 1340-1344, 2000.

[13] A. Burr, "Evaluation of capacity of indoor wireless MIMO channeling using ray tracing," *IEEE International Seminar on Broadband Communication*, pp. 28-1 – 28-6, 2002.

[14] V. Pohl, V. Jungnickel, T. Haustein, and C.V. Helmolt, "Antenna spacing in MIMO indoor channels," *IEEE Vehicular Technology Conference*, vol.2, pp. 749-753, Spring 2002.

[15] S.R. Saunders, *Antennas and propagation for wireless communication systems*, Wiley, 1999.

[16] M.C. Lawton, J.P. McGeehan, "The application of a deterministic ray launching algorithm for the prediction of radio channel characteristics in small-cell environment," *IEEE Trans. Vehicular Technology*, vol. 43, pp. 955-969, Nov. 1994.

[17] M. Haardt, and J.A. Nossek, "Unitary ESPRIT: How to obtain increased estimation accuracy with a reduced computational burden," *IEEE Trans. Signal Processing*, vol.43, pp. 1232-1242. May 1995.

[18] M. Haardt, and J.A. Nossek, "Simultaneous Schur decomposition of several nonsymmetric matrices to achieve automatic pairing in multi-dimensional harmonic retrieval problems." *IEEE Trans. Signal Processing*, vol. 46, pp. 161-169. Jan. 1998.